sider the measured pressures and temperatures. These values enable the quantities T_h/T_c, Kn_{cl}, and Kn_{cs} to be calculated. From Knudsen's results, it seems reasonable to assume that $p_c = p_h$ when $Kn_c \leqslant 0.01$, or $p_{cl} = p_{hs} = p_h$. Therefore, at each temperature ratio T_h/T_c, the ratio of p_{cs}/p_h may be calculated for a range of values of Kn_{cs} up to the point where $Kn_{cl} = 0.01$. When $Kn_{cl} \geqslant 0.01$, then p_{cl}/p_h is given by the experimentally determined variation of p_{cs}/p_h with Kn_{cs} which was determined when Kn_{cl} was still less than 0.01. Therefore, when p_{cl} is known, p_h and p_{cs}/p_h can be calculated. Thus, by using this bootstrap technique, the relationship between p_{cs}/p_h may be extended to large values of Kn_c.

An example of the results of the experiments is shown in Fig. 2. It can be seen that, up to a Knudsen number of five, the degree of scatter in the data is very small. Since

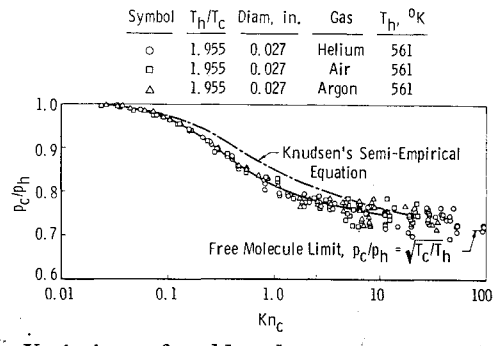

Fig. 2 Variation of cold-to-hot pressure ratio with Knudsen number (cold).

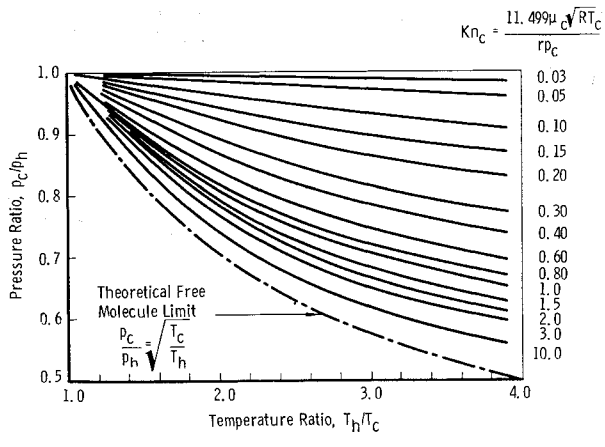

Fig. 3 A working chart to correct for thermomolecular pressure effects in tubes (gage at the cold end).

this test involved the use of three different gases (air, argon, and helium), the results tend to confirm the validity of using Knudsen number as a correlating parameter. For Knudsen numbers greater than five, the degree of scatter increases to approximately ±5% (±0.5 μ Hg in these tests) about a mean curve through the experimental data. Despite this degree of scatter, it seems reasonable to conclude that the limiting value of p_c/p_h predicted by Eq. (1) is attained at a sufficiently large Knudsen number. Furthermore, it will be noted that there is some disagreement between the values predicted by Knudsen's semiempirical equation and the present results. Knudsen's curve was derived on the basis of data for a temperature ratio of 1.07. He did, in fact, carry out some tests at a temperature ratio of approximately two and found that his semiempirical equation did not predict exactly the measured values.

The temperature ratio covered in the author's experiments ranges from 1.5 to 3.8. Using these results, a working chart permitting the calculation of the temperature effect on pressure is given in Fig. 3.

References

[1] Knudsen, M., "Thermischer Molekulardruck in Röhren," Ann. Physik **83**, 797–821 (1927).

[2] Howard, W. M., "An experimental investigation of pressure gradients due to temperature gradients in small diameter tubes," Guggenheim Aeronaut. Lab., Calif. Inst. Tech., Pasadena, Calif., Memo. 27 (June 10, 1955).

[3] Arney, G. D., Jr. and Bailey, A. B., "An investigation of the equilibrium pressure along unequally heated tubes," Arnold Eng. Dev. Center TDR-62-26 (February 1962).

[4] Arney, G. D., Jr. and Bailey, A. B., "Addendum to an investigation of the equilibrium pressure along unequally heated tubes," Arnold Eng. Dev. Center TDR-62-188 (October 1962).

Viscous Interaction Effects on a Static Pressure Probe at $M = 6$

WILHELM BEHRENS*
California Institute of Technology, Pasadena, Calif.

The purpose of this investigation was to find the relation between measured static pressure and true static pressure as a function of the viscous interaction parameter $\bar{\chi}$. The results obtained make possible accurate interpretation of measured static pressure data.

1. Design of Pitot-Static Probe

THE dimensions of the static pressure probe were chosen so that the measured value of the static pressure was as close as possible to the freestream static pressure. Using the data of Matthews,[1] three pressure orifices were located 10 diameters behind the shoulder of a tube with a 20° cone tip. The length of the uniform-diameter tube section behind the pressure orifices was chosen to be 20 boundary-layer thicknesses (calculated at the location of the orifices, for the lowest operating pressure). A sketch of the probe is shown in Fig. 1.

2. Measurements and Data Reduction

The pitot pressures were measured with a Welch mercury manometer and the static pressures with a silicone U-tube manometer. The total pressures were measured by means of a Tate-Emery pressure indicator. The static pressures of the freestream were computed from the pitot and total pressures using the isentropic flow relations. The accuracy of the pitot pressure measurements was estimated to ±0.2%, and that of the total pressure was ±0.1%, so that the "correct" static pressures were accurate to about ±0.3%. The accuracy of the pressure measured with the static probe was also about ±0.3%. During all tests, the total temperature was maintained at 300°F. (At a total temperature of 234°F and for pressures greater than 50 psig, inconsistent results were obtained, which were traced to condensation effects.) Measurements were taken at total pressures ranging from 8 to 100 psig. The experimental data obtained are plotted in Fig. 2 in terms of the ratio (p_m/p_∞), where p_m is the measured pressure and p_∞ is the "correct" static pressure.

Received September 3, 1963. The work discussed in this paper was carried out under the sponsorship and with the financial support of the U. S. Army Research Office and the Advanced Research Projects Agency, Contract No. DA-31-124-ARO(D)-33. This research is a part of Project Defender sponsored by the Advanced Research Projects Agency.

* NATO Graduate Fellow, Department of Aeronautics, Firestone Flight Sciences Laboratory, Graduate Aeronautical Laboratories.

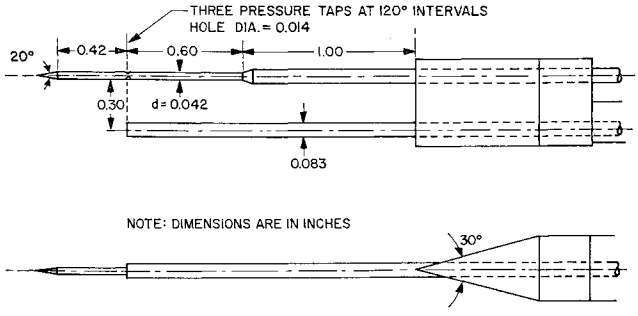

Fig. 1 Pitot-static probe.

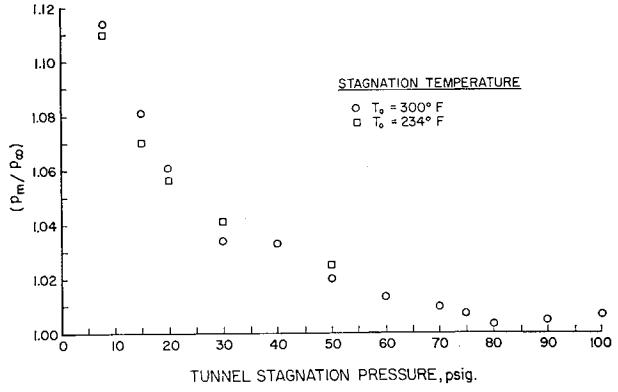

Fig. 2 Static pressure ratio vs total pressure.

3. Relation for Correction of Static Pressure Data

For weak hypersonic viscous interaction, the following formula relating the measured and the original, or inviscid static, pressure is given by Hayes and Probstein[2]:

$$(p_m/p_{\text{orig}}) - 1 = A\bar{\chi} + B\bar{\chi}^2$$

where

$$\bar{\chi} = \frac{M_{\text{orig}}{}^3 C_{\text{orig}}{}^{1/2}}{(Re_{x\ \text{orig}})^{1/2}}$$

is the viscous interaction parameter, and where

$$C_{\text{orig}} = (\mu_w/\mu_{\text{orig}})(T_{\text{orig}}/T_w)$$

and the subscripts orig and m denote inviscid and measured values, respectively, on the body at the station x, where x is measured from its tip; A and B are constants to be determined. This formula is an expansion for small $\bar{\chi}$ which has been found to be valid for flat plates[2] and cones.[3] It is expected that a similar relation holds for a cone-cylinder body.

The inviscid flow data were computed for the cone-cylinder model shown in Fig. 1. The cone angle is 20°, and the static pressure holes are located 12.84 d behind the tip of the probe (= 10 d behind the shoulder). The values shown in Table 1 at this station were obtained from Ref. 4 by interpolation. Hence, the static temperature T and the Mach number at 10 d behind the shoulder of the cone-cylinder are practically equal to the freestream values. The static pressure and the density on the probe deviate from the freestream conditions; their values can be obtained from Fig. 3.

Figure 2 presents the measured static pressure as a function of the tunnel total pressure. To relate these data in a more significant way, the measured static pressure p_m divided by the theoretical inviscid pressure p_{orig} was plotted in Fig. 4

Table 1 Inviscid flow data at orifice location of static probe

M_∞	(p/p_∞)	M	(T/T_∞)	(ρ/ρ_∞)
6	0.948	5.974	1.006	0.942

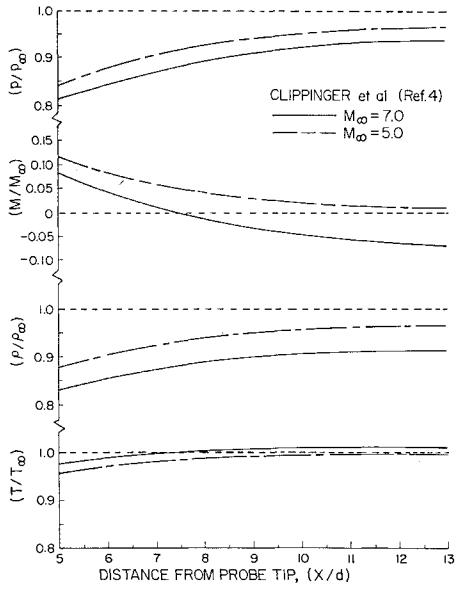

Fig. 3 Inviscid flow about a 10° half-angle cone-cylinder.

against the viscous interaction parameter $\bar{\chi}$. The empirical relation obtained in this fashion is

$$(p_m/p_{\text{orig}}) - 1 = 0.065\bar{\chi} + 0.04\bar{\chi}^2$$

In comparison, the viscous interaction results for flat plates and cones are quoted. For flat plates in air[2] (γ = 1.4), this relation is

$$(p_m/p_{\text{orig}}) - 1 = 0.31\bar{\chi} + 0.05\bar{\chi}^2$$

To the first order in $\bar{\chi}$, the equation for slender cones given by hypersonic viscous interaction theory is[3]

$$(p_m/p_{\text{orig}}) - 1 = 0.142\bar{\chi}$$

The experimental cone values are correlated by the relation[3]

$$(p_m/p_{\text{orig}}) - 1 = 0.124\bar{\chi}$$

These results demonstrate that the viscous interaction for the cone-cylinder is quite small compared to that of the flat plate and the semi-infinite cone.

Matthews[1] obtained the pressure distribution along a probe with a cone half-angle of 10° and a diameter of 0.083 in. at a constant total pressure of 88.4 psia. The measured pressures were somewhat higher than those found in the present investigation (see Fig. 4). The important parameters of the problem are the angle of expansion, the distance of the static pressure orifice from the expansion corner (in diameters), and the Reynolds number based on probe diameter. When the Reynolds number becomes small, the effect of the transverse curvature of the boundary layer on the cone-cylinder becomes important. The boundary-layer thickness of the probe at the point where the static holes are located was computed by the method of Timman[5] and found to be about two-thirds the thickness of an equivalent

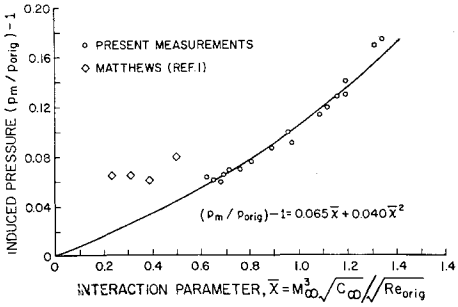

Fig. 4 Viscous interaction on a cone-cylinder probe.

flat plate boundary layer. It is of the order of the probe diameter. In laminar incompressible boundary layers, the displacement thickness δ^* of an axisymmetric paraboloid is[6]

$$(\delta^*/x) = 0\{1/[(Re_x)ei(Re_L)]^{1/2}\}$$

where L is the focal length, x the distance from the tip of the body, and

$$ei(Re_L) = \int_{Re_L}^{\infty}\left[\frac{(e^{-\eta})}{\eta}\right]d\eta \cong -0.5772 + \ln\left(\frac{1}{Re_L}\right) + Re_L - \left(\frac{Re_L^2}{2\cdot 2!}\right) + \ldots$$

for small Reynolds numbers Re_L. This relation shows that the smaller the L, and therefore the smaller the diameter, the smaller is the ratio of displacement thickness δ^* to x. This behavior of δ^* seems to be one essential cause of the comparatively small interaction results obtained. To obtain a more detailed understanding of the flow field, additional theoretical and experimental investigations are necessary. However, the present results can be used for the reduction of static pressure measurements, obtained using static probes similar to the one given in Fig. 1.

References

[1] Matthews, M. L., "An experimental investigation of viscous effects on static and impact pressure probes in hypersonic flow," Graduate Aeronaut. Labs., Calif. Inst. Tech., Hypersonic Research Project, Memo. 44 (June 2, 1958).

[2] Hayes, W. D. and Probstein, R. F., *Hypersonic Flow Theory* (Academic Press, New York and London, 1959), Chap. IX.

[3] Talbot, L., Koga, T., and Sherman, P. M., "Hypersonic viscous flow over slender cones," NACA TN 4327 (September 1958).

[4] Clippinger, R. F., Giese, T. H., and Carter, W. C., "Tables of supersonic flows about cone cylinders. Part I: Surface data," Ballistic Res. Labs. Rept. 729 (October 15, 1960).

[5] Timman, K., "Hypersonic flow about a thin body of revolution," AGARD Rept. 141 (July 1957).

[6] Mark, R. M., "Laminar boundary layers on slender bodies of revolution in axial flow," Graduate Aeronaut. Labs., Calif. Inst. Tech., Hypersonic Research Project, Memo. 21 (July 30, 1954).

Gyro Torquing Signals at an Arbitrary Azimuth on an Ellipsoidal Earth

Myron Kayton*

Litton Industries, Woodland Hills, Calif.

THIS note shows the exact expressions for gyro torquing signals in a wander-azimuth system. It is not intended as a general discussion of wander-azimuth mechanizations. The use of a wandering azimuth requires special computation provisions for generating α.

Consider a vehicle at P, Fig. 1, moving near the surface of the earth at a velocity $\bar{V}$ (not necessarily horizontal). The arc DCE is a worldwide reference ellipsoid representing the earth, and $ABCP$ is the normal to the ellipsoid which passes through P. $CP = h$ is the height of the vehicle above the ellipsoid, and ϕ is the geographic latitude of the vehicle. The relevant dimensions of the ellipsoid are its semimajor axis a and its eccentricity ϵ [not to be confused with the flattening or ellipticity, $f = 1 - (1 - \epsilon^2)^{1/2} \approx \epsilon^2/2$].

Received September 3, 1963.

* Senior Research Engineer, Guidance and Control Systems Division. Member AIAA.

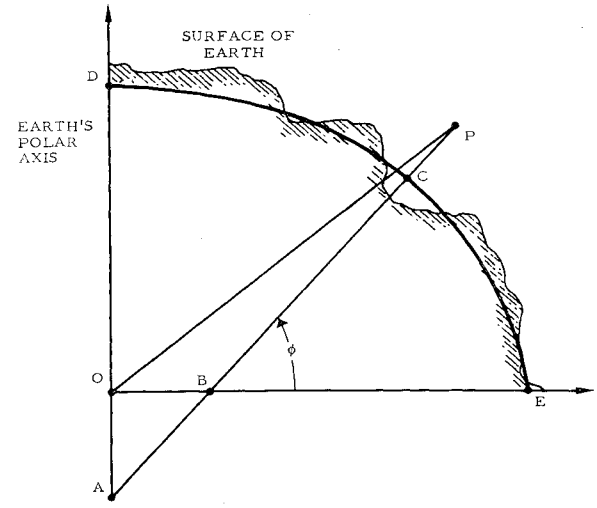

Fig. 1 Meridian section of reference ellipsoid.

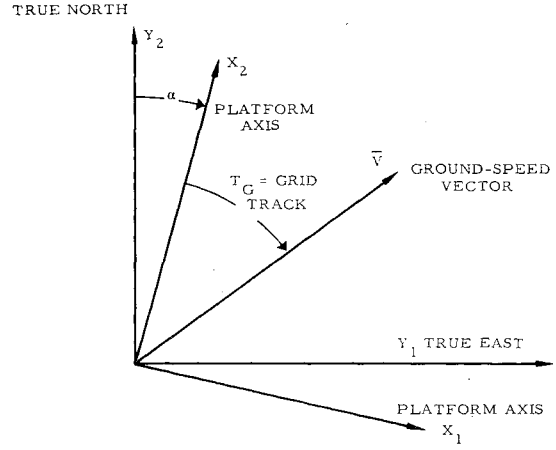

Fig. 2 Plan view of level platform at an azimuth α.

The vehicle is assumed to carry an inertial platform whose orthogonal torquer axes define the coordinate frame $x_1x_2x_3$. The platform is locally level (x_3 lies along $ABCP$ and points upward) and oriented with its x_2 axis at an azimuth α from north (Fig. 2). A horizontal plane at any altitude is here defined as a plane perpendicular to the projected normal to the ellipsoid, $ABCP$.

A non-north azimuth orientation is used for many purposes:

1) It can allow the use of a transverse pole, on the earth's equator, to permit operation near the true poles.

2) It can allow the use of redundant coordinates, such as direction cosines, to permit operation at all latitudes.

3) It can eliminate the Coriolis correction or maintain a constant azimuth torque rate, independent of vehicle speed.

The basic mechanization equations for an aircraft or ship inertial navigator are[1]

$$d\bar{V}/dt]_p = \bar{f} + (\bar{\omega}_{EP} + 2\bar{\Omega}) \times \bar{V} - g \qquad (1)$$

where

$\bar{f}$ = accelerometer output, expressed as an acceleration

$\bar{\omega}_{EP}$ = desired angular velocity of platform relative to the earth

$\bar{\Omega}$ = earth's inertial angular velocity

$d\bar{V}/dt]_p$ = time derivative of $\bar{V}$ in platform axes

$\bar{g}$ = gravity (not Newtonian gravitation $\bar{G}$). The horizontal component of $\bar{g}$ (tangent to the reference ellipsoid) is zero, neglecting local anomalies, at all altitudes below 35 naut miles